Ultrafast Dynamics in Biological Systems and in Nano-Confined Environments

Kalyanasis Sahu, Sudip Kumar Mondal, Subhadip Ghosh, and Kankan Bhattacharyya*

Physical Chemistry Department, Indian Association for the Cultivation of Science, Jadavpur, Kolkata 700 032, India

Received December 28, 2006; E-mail: pckb@mahendra.iacs.res.in

Ultrafast chemical dynamics in a nano-confined system is very different from that in a bulk liquid. In this account, we give an overview on recent femtosecond study on dynamics of ultrafast chemical processes in the nanocavity of a biological system. Dynamics in a biological system crucially depends on the location of the fluorescent probe. We show that one can study solvation dynamics in different regions (i.e. spatially resolve) by variation of the excitation wavelength. We discuss two interesting cases of how structure affects dynamics. First, solvation dynamics of two protein folding intermediates of cytochrome *c* is found to be differ significantly in the ultrafast initial part (<20 ps). Second, methyl substitution of the OH group in a cyclodextrin is shown to slow down the initial part of solvation dynamics quite dramatically. The most interesting observation is the discovery of the ultraslow component of solvation dynamics which is 100–1000 times slower compared to bulk water. The electron- and proton-transfer processes in a nano-confined system are found to be markedly retarded because of slow solvation and structural constraints. Close proximity of the reactants in a confined system is expected to accelerate dynamics of bi-molecular processes. This is illustrated by ultrafast fluorescence resonance energy transfer (FRET) in ≈1 ps time scale between a donor and an acceptor in a micelle. Finally, it is demonstrated that the decay of fluorescence anisotropy provides structural information (e.g. size of a cyclodextrin inclusion complex) and may be used to detect formation of a nano-aggregate.

1. Introduction

Many natural and biological processes occur in a nano-confined environment. In such a system, the reactive species along with several solvent molecules remain confined in a nanocavity. The common examples of a confined system are hydrophobic pocket of a protein (enzyme), minor/major grooves or interior of a DNA double helix, micelles or lipids, and nano-cavities of many supramolecules involving cyclodextrin or other hosts. In an aqueous solution, such a nano-cavity is spontaneously created through self-assembly of amphiphilic molecules and originates from a delicate balance of hydrophobic and hydrophilic interactions. Structure of these assemblies has been studied by many techniques. In contrast, dynamics in these systems is relatively unexplored. There is a long standing interest to elucidate dynamics in a nano-confined system and eventually, its role in the function of a biological system. Recently, significant progress towards this end has been made using ultrafast femtosecond spectroscopy and large scale computer simulations. The local properties of a "nano-liquid" (i.e. a liquid confined in a nanocavity) differ in a number of ways from those in a bulk liquid. In general, polarity of a nano-confined liquid is much lower than that in the bulk. Also, dynamics of most chemical processes in a nano-confined liquid is markedly slower compared to a bulk liquid because of local constraints. In this account, we will give a brief overview of some ultrafast processes in a wide range of nano-cavities.

We begin with solvation dynamics of "biological water" (i.e. water molecules confined in a biological system), in Section **2**. We show that biological water displays an ultraslow component of solvation dynamics in 100–1000 ps time scale which is slower by 2–3 orders of magnitude compared to bulk water. In Section **3**, we will discuss how the ultraslow solvation dynamics affects excited state proton- and electron-transfer processes. Bi-molecular reactions are expected to be very fast in a confined system because of the close proximity of the reactants. In Section **4**, we illustrate this with fluorescence resonance energy transfer (FRET) in a micelle and a reverse micelle. Finally, in Section **5**, we will give an overview of some recent applications of fluorescence anisotropy decay in confined environments.

2. Solvation Dynamics

Solvation dynamics refers to the dynamic response of a set of polar solvent molecules towards a dipole suddenly created by excitation of a solute using an ultrashort laser pulse. For this experiment, one chooses a solute (probe) whose dipole moment is very small in the ground state but is very large in the excited state. The dynamic response of the solvent molecules is not instantaneous. With increase in time, the solvent

Published on the web June 13, 2007; doi:10.1246/bcsj.80.1033

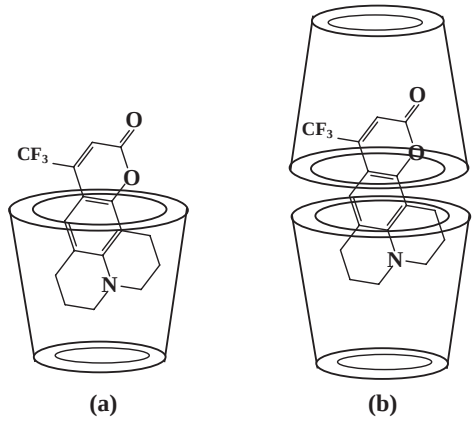

Fig. 1. (a) 1:1 and (b) 1:2 complexes of C153 with methyl-β-cyclodextrin.

molecules gradually rearrange and reorient around the dipole in the excited state and thus, energy of the excited dipole decreases. The energy relaxation is manifested in a time-dependent red shift of the emission spectrum. This phenomenon is known as dynamic Stokes shift. In the case of solvation dynamics, the fluorescence decay exhibits a marked dependence on the wavelength. At a short emission wavelength, a decay is observed which arises mainly from the unsolvated species. At a very long wavelength, where emission from the solvated species predominates, a rise precedes the decay. The rise at a long wavelength is a clear manifestation of solvation dynamics. The gradual change in solvation (i.e. solvation dynamics) is monitored by the decay of the solvation time correlation function, $C(t)$ which is defined as

$$C(t) = \frac{\nu(t) - \nu(\infty)}{\nu(0) - \nu(\infty)}, \quad (1)$$

where, $\nu(0)$, $\nu(t)$, and $\nu(\infty)$ are the observed emission frequencies at time zero, t, and infinity, respectively.

Solvation dynamics in bulk water is described by a major component in 0.1 ps (100 fs) time scale and a minor component of 1 ps.[1–4] Interestingly, solvation dynamics of water confined in many organized and biological assemblies displays a component in 100–1000 ps time scale.[5–9] The ultraslow component of solvation dynamics suggests that nano-confined water ("biological water") is substantially slower and fundamentally different from ordinary water. Many aspects of ultraslow biological water have been reviewed earlier.[5–8] In this account, we focus only on the latest results.

2.1 Solvation Dynamics in a Cyclodextrin Nanocage. A cyclodextrin is a cyclic polymer containing 6–8 glucose units which is soluble in water and in many other polar liquids. In a cyclodextrin (CD) nanocavity, an organic fluorescent probe may be confined along with several (≈10) solvent molecules (Fig. 1). Compared to the unsubstituted CD-s, the *O*-methyl or *O*-hydroxypropyl derivatives are much more soluble in water. The higher solubility of the substituted CD's finds useful application in targeted delivery of drugs which are sparingly soluble in water[10] and also, prevents misfolding and aggregation of proteins by encapsulating its aromatic residues.[11]

Fleming and co-workers first reported that solvation dynamics of water is dramatically slowed down inside an unsubstituted cyclodextrin cavity and displays a component as slow as 109 and 1200 ps.[12] They suggested three possible sources for the ultraslow component—the restricted motion of the confined water molecules, motion of the guest (probe) in and out of the cavity, and third, the fluctuations of the γ-cyclodextrin ring. Recently, Sen et al. studied the effect of methyl substitution of cyclodextrin on ultrafast solvation dynamics.[13] In trimethyl β-CD, all the three OH groups of the β-CD cavity are replaced by OMe groups. It is observed that solvation dynamics in trimethyl β-CD displays two very slow components—240 ps (45%) and 2450 ps (31%) along with a fast component of 10 ps (24%) (Fig. 2).[13] This is significantly slower than the solvation dynamics in an un-substituted cyclodextrin. In contrast, dimethyl β-CD (which contains one OH group per glucose unit) exhibits extremely fast dynamics with a major (40%) ultrafast component (<0.3 ps), a fast component of 2.4 ps (24%), and two slow components—50 ps (18%) and 1450 ps (18%) (Fig. 2).

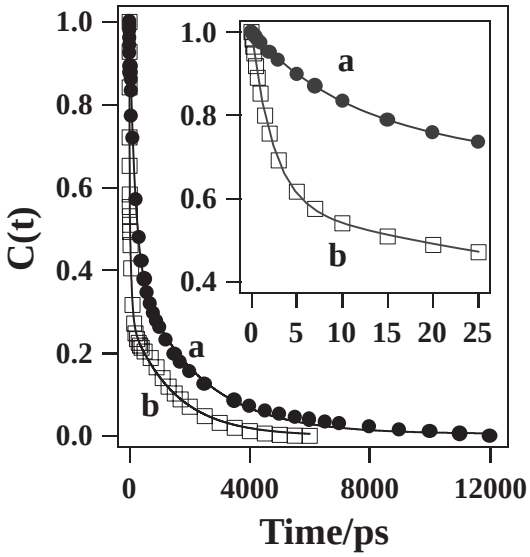

Fig. 2. Decay of response function, $C(t)$ of C153 bound to (a) 130 mM trimethyl β-CD (●) and (b) 130 mM dimethyl β-CD (□) in water. The points denote the actual values of $C(t)$ and the solid line denotes the best fit to an exponential decay. Initial parts of the decays of $C(t)$ are shown in the inset (Reprinted with permission from Ref. 13. Copyright © 2005 American Chemical Society).

The surprisingly slow dynamics in trimethyl β-CD is explained as follows. In bulk water, ultrafast solvation dynamics arises from the extended hydrogen-bonded network.[4] In the case of unsubstituted CD-s, similar network is established between the water molecules inside the cavity with those outside the cavity through the OH group of the cyclodextrins. Hence, a major part of solvation dynamics in an unsubstituted cyclodextrin is ultrafast (<2 ps). In the case of trimethyl β-CD, there are no OH groups at the rim of the cyclodextrin cavity. Thus, there is no hydrogen-bond network connecting the water molecules inside the cyclodextrin cavity and those outside the cavity. As a result, the ultrafast component (≤2 ps) vanishes almost completely in trimethyl β-CD. Because of the presence of seven OH groups at the rim of dimethyl β-CD, the hydrogen-bond network is at least partially established. Thus in this

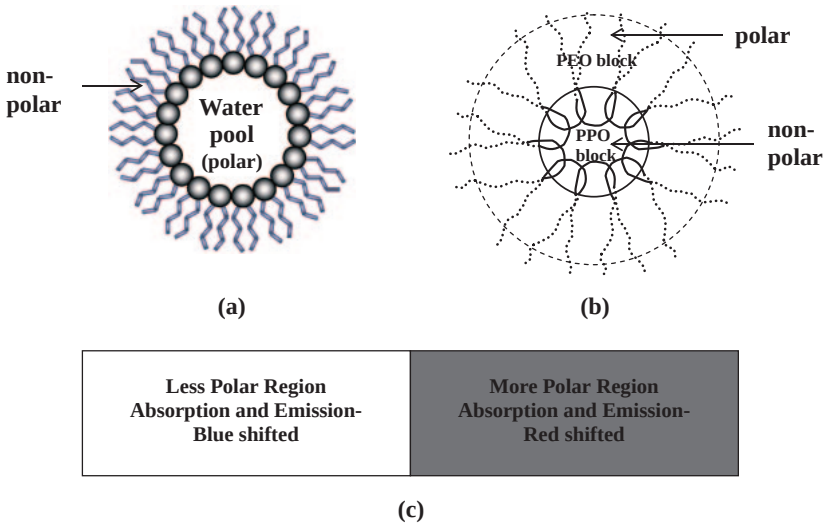

Fig. 3. (a) AOT reverse micelle, (b) P123 micelle with a non-polar core (PPO block) and polar corona (PEO block), and (c) schematic representation of polar and non-polar regions.

case, there is a major (64%) ultrafast component ($\leq$0.3 and 2.4 ps) of solvation dynamics.

2.2 Excitation Wavelength Dependence and Spatially Resolved Dynamics. In this section, we discuss how one can spatially resolve dynamics in an organized assembly i.e. study dynamics in different regions. In an organized assembly, the polarity and hence, the absorption and emission maxima of a probe are different in different regions (Fig. 3). Consequently, the probe molecules in different locations of an organized assembly may be selectively excited by varying the excitation wavelength (λ_{ex}). At a short wavelength ("blue edge") the probe molecules in a relatively nonpolar environment are excited and this gives rise to a blue-shifted emission spectrum. Excitation at a longer wavelength ("red edge") selects the probe in a relatively polar environment and gives rise to a red-shifted emission spectrum. Such an excitation wavelength dependence of emission maximum is known as red edge excitation shift (REES).[14–16]

Satoh et al. investigated λ_{ex} dependence of solvation dynamics of coumarin 343 (C343) in the water pool of an AOT (aerosol-OT) reverse micelle (Fig. 3a) using a picosecond set up.[17] They observed that the observed dynamic Stokes shift ($\Delta\nu$) decreases with increase in the excitation wavelength. To explain this it is proposed that the probe molecules are distributed broadly over two environments. The first environment is a bulk-water-like region in the core of water pool where solvation dynamics occurs on a sub-100 ps time scale. The other is a region in the vicinity of the surfactant head-group where the dynamics is much slower (700 and 2000 ps). Excitation at the red end of the absorption spectrum preferentially selects the probes in the bulk-like region. The sub-100 picosecond dynamics in Stokes shift in this region remains undetected in a picosecond set up and hence, $\Delta\nu$ decreases with increase in λ_{ex}.

In a lipid vesicle, a highly hydrophobic bilayer membrane encloses a polar water pool. Sen et al. studied λ_{ex} dependence of solvation dynamics of coumarin 480 (C480) in a DMPC ((dimyristoyl)phosphatidylcholine) vesicle using a picosecond[18] and a femtosecond[19] set up. For λ_{ex} = 390–430 nm, solvation dynamics in a lipid displays an ultrafast component (<0.3 ps) and a fast component (1.5 ps) along with two slow components—250 and 2000 ps. With increase in λ_{ex}, the relative contribution of the ultrafast components (<0.3 and 1.5 ps) increases from 48% at λ_{ex} = 390 nm to 100% at λ_{ex} = 430 nm. Thus, at λ_{ex} = 430 nm, there is no slow component (Fig. 4). The ultrafast dynamics is ascribed to the very polar and mobile bulk-like region, deep inside the water pool. The slow dynamics (250 and 2000 ps) arises from a restricted interfacial region inside the bi-layer membrane.

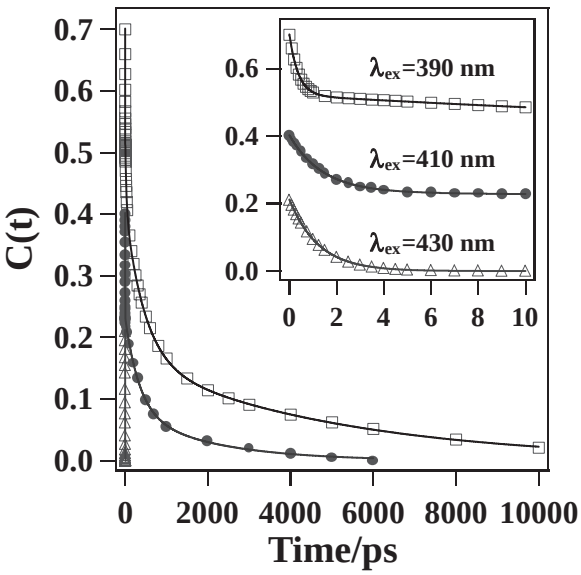

Fig. 4. Decay curves of $C(t)$ of C480 in DMPC vesicle for λ_{ex} = 390 nm (□), λ_{ex} = 410 nm (●), and λ_{ex} = 430 nm (△). The initial portions of the decay curves are shown in the inset (Reprinted with permission from Ref. 19. Copyright © 2006 Wiley-VCH Verlag GmbH & Co. KGaA, Weinheim).

A tri-block co-polymer micelle (e.g. PEO_{20}–PPO_{70}–PEO_{20}, Pluronic P123) consists of a slow, hydrophobic and nonpolar PPO (poly(propylene oxide)) core and a polar, fast bulk-like

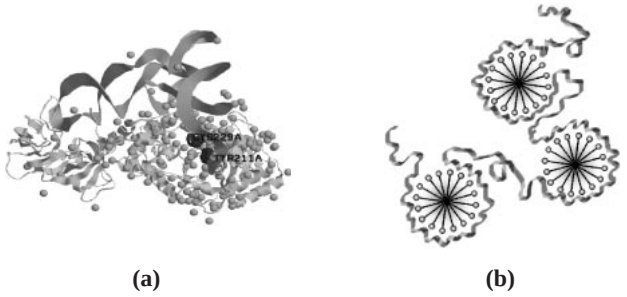

(a) (b)

Fig. 5. (a) Structure of GlnRs (PDB entry 1QTQ), (b) necklace model of protein–surfactant (cytochrome *c*–SDS) aggregate.

peripheral corona containing the PEO (poly(ethylene oxide)) block (Fig. 3b). Sen et al. studied solvation dynamics in different regions of a P123 micelle by varying λ_{ex}.[20] With increase in λ_{ex} from 375 to 478 nm, the emission maximum of C480 exhibits a large red edge excitation shift (REES) by 25 nm. With increase in λ_{ex}, solvation dynamics in P123 micelle becomes faster. The λ_{ex} dependence in P123 micelle has been interpreted in terms of three regions—the fast PEO-water interface with solvation time $\leq$2 ps, chain region (60 ps), and a very slow (4500 ps) hydrophobic core region (PPO–PEO interface). With increase in λ_{ex}, contribution of the bulk-like ultrafast dynamics ($\leq$2 ps) increases from 7% at $\lambda_{ex} = 375$ nm to 78% at $\lambda_{ex} = 425$ nm. There is a concomitant decrease in the contribution of the core-like slow component (4500 ps) from 79% at $\lambda_{ex} = 375$ nm to 17% at 425 nm.[20] Contribution of the of 60 ps component, which arises from chain dynamics, decreases from 14% at $\lambda_{ex} = 375$ nm to 5% at $\lambda_{ex} = 425$ nm.[20]

2.3 Solvation Dynamics in Proteins and DNA. The biological function of a protein is largely controlled by the quasi-bound biological or structured water molecules at the surface.[5–9] Guha et al.[21] studied solvation dynamics at the active site of an enzyme, glutaminyl-tRNA synthetase (GlnRS) (Fig. 5). For this purpose, they attached a fluorescence probe, acrylodan, at a cysteine residue C229, near the active site. Solvation dynamics in GlnRs displays two slow components—400 and 2000 ps. When the amino acid glutamine (Gln) binds to the enzyme (GlnRS) the 400 ps component slows down about 2-fold to 750 ps while the 2000 ps component remains unchanged. When $tRNA^{gln}$ binds to GlnRS the 400 ps component does not change but the 2000 ps component becomes slower (2500 ps). From this, it is inferred that the 400 ps component arises from the water molecules at the Gln binding site while the 2000 ps corresponds to the $tRNA^{gln}$ binding site. A mutant Y211H-GlnRS was constructed in which the glutamine binding site is disrupted. The mutant Y211H-GlnRS labeled at C229 with acrylodan exhibits significantly different solvent relaxation.[21] This demonstrates that the slow dynamics is indeed associated with the active site.

The mitochondrial respiratory membrane protein cytochrome *c* is cationic in nature and carries a net positive charge (+8) at a neutral pH ($\approx$7). Binding of cytochrome *c* to anionic surfactants (e.g. sodium dodecyl sulfate, SDS) or membranes results in partially folded or molten globule-like states (Fig. 5). Cytochrome *c* forms two partially folded intermediates—I_1 (in the presence of SDS) and I_2 (in the presence of

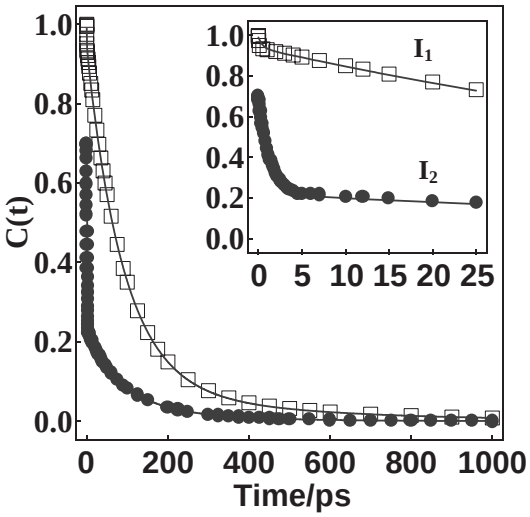

Fig. 6. Initial part of the decay of $C(t)$ of C153 containing 5 μM cytochrome *c* and 2 mM SDS (I_1) (□); 5 μM cytochrome *c*, 2 mM SDS and 5 M urea (I_2) (●) (Reprinted with permission from Ref. 23. Copyright © 2006 American Chemical Society).

SDS and urea).[22] Solvation dynamics in these two partially folded states of cytochrome *c* are found to be drastically different and the most prominent differences are detected at very early times (<20 ps, Fig. 6).[23] I_1 displays an ultrafast component—0.5 ps (5%), and two slow components—90 ps (85%) and 400 ps (10%). In the case of I_2, there is a major ultrafast component of 1.3 ps (47%) and two slow components—60 ps (12.5%) and 170 ps (10.5%). The faster solvation dynamics suggests that I_2 is more open and labile compared to I_1.[23] Samaddar et al. studied solvation dynamics in the pre-molten globule state of GlnRS.[24] They observed that the solvation time is of the order, native > molten globule > premolten globule.

Sen et al. studied solvation dynamics in hen egg white lysozyme in the presence of urea and SDS using coumarin 153 (C153) as a probe.[25] They found that a small amount of SDS (3 mM) causes partial recovery of the urea denatured protein and solvation dynamics in this system is very close to that in the native protein. However, large excess of SDS (28 mM) causes complete loss of the tertiary structure of the native protein and the SDS micelles are squeezed inside the polypeptide chain of the protein. This results in a 3.5 times retardation of solvation dynamics compared to that in the native state.[25] Sahu et al. studied interaction of a cationic surfactant cetyltrimethylammonium bromide (CTAB) with the cationic protein lysozyme.[26] In this case, hydrophobic interaction dominates over the electrostatic repulsion between the cationic protein and the cationic surfactant. Solvation dynamics in a lysozyme–CTAB aggregate is much slower than that in a CTAB micelle or in the protein (lysozyme).[26]

Very recently, several groups have applied large scale molecular dynamics simulations to elucidate solvation dynamics in different regions of a protein. Bagchi and co-workers investigated solvation dynamics in a 36-residue globular protein, HP-36.[27,28] The secondary structure of this protein contains three short alpha-helices. The solvation dynamics of the polar

amino acid residues in helix-2 ($\langle\tau\rangle = 11$ ps) is found to be 2-fold faster than that in the other two helices. Surprisingly, the water molecules around helix-2 exhibit much slower orientational dynamics than those around the other two helices. It is shown that the dynamics depends on the degree of exposure. An exposed water molecule displays fast solvation dynamics while a buried one exhibits slower dynamics.[28]

Marchi and co-workers studied folding of a zwitterionic alanine octapeptide (A_8) in a reverse micelle (RM) by MD (molecular dynamics) simulation.[29] They showed that in the confined environment (RM), the folded structure of a protein is much more stable than the unfolded structure.[29] For a small RM, a stable helical structure of the polypeptide is detected. With rise in water content (w_0) as the size of water pool increases, the polypeptide forms an extended structure.[29] In a MD simulation, Zhong and co-workers detected multiple time scales of solvent relaxation in a peptide from femtosecond to tens of picoseconds.[30] Using terahertz spectroscopy and simulation, Heugen et al. showed that water molecules near a biomolecule (lactose) are markedly slow.[31] They found that the hydration layer around the carbohydrate extends up to 5.13 Å from the surface and contains 123 water molecules.[31]

In contrast to the large body of work demonstrating ultraslow dynamics near a protein, incoherent quasi-elastic neutron scattering[32,33] and NMRD (nuclear magnetic relaxation dispersion)[34] studies suggest very slight slowing down of the water molecules near a protein. It may be noted that different techniques detect different things. First, dielectric relaxation (DR) and dynamic Stokes shift capture collective response of the solvent (water) dipoles. NMRD and QENS (quasi elastic neutron scattering) describe dynamics of a single water molecule in the absence of an electric field (i.e. in an equilibrium situation). Second, NMRD, QENS, and DR offer no spatial resolution and all the water molecules contribute in these experiments. Dynamic Stokes shift, however, is dominated by the water molecules in the first solvation shell and thus, has a high spatial resolution. Evidently, the number of quasi-bound water molecules around a fluorescent probe is very small compared to the very large number of water molecules present around a protein. NMRD and QENS data are dominated by the huge number of water molecules, many of which are very fast (particularly those at the surface of a protein). Thus, NMRD and QENS which detect an average of the water molecules at all the sites, often report very fast dynamics or almost bulk-water-like residence times with very small (sometimes negligible) contribution of the slow water molecules. In contrast, dynamic Stokes shift reports predominantly the dynamics of the slow and buried water molecules in deep, hydrophobic pockets and hence, detect a relaxation component which is markedly slower compared to bulk water.

Most recently, many groups have studied dynamic Stokes shift in DNA.[35–37] Zewail and co-workers studied solvation dynamics in DNA using 2-aminopurine as an intrinsic probe and a minor groove binding non-covalent probe, pentamidine.[35] They detected a bi-exponential decay with an ultrafast subpicosecond component due to bulk water and a relatively long ($\approx$10 ps) component. Berg and co-workers studied a series of oligo-nucleotides in which a native base pair is replaced by a dye molecule (C480).[36] They found that when the probe (C480) is in the centre of the helix, the time scale of relaxation is broadly distributed over six decades of time scale from 40 fs to 40 ns and obeys a power-law, $(1 + \tau/\tau_0)^{-\alpha}$. The very long ($\approx$40 ns) component is assigned to the reorganization dynamics of DNA. Since the interior of the double-helix is devoid of water, the observed Stokes shift seems to originate from the electric field of DNA on the probe. When the probe (C480) is attached at the end of the helix an additional very fast component of 5 ps is detected.[37] The 5 ps component and the increased mobility ("fraying") at the end of the helix is ascribed to increased exposure of the probe to bulk water and lower counter ion concentration.[37]

2.4 Origin of Ultraslow Dynamics of Biological Water. We now discuss a phenomenological model which explains the slow dynamics of the "biological water." According to Nandi and Bagchi[9] in an organized assembly, the dielectrics response arises from two kinds of water molecules—"bound" and "free." The "bound" water molecule are those which are hydrogen bonded to a large biological macromolecule and immobilized losing their translational and rotational degrees of freedom. The free water molecules are hydrogen bonded to other water molecules and retain bulk-like ultrafast mobility. The bound state of water is usually lower in energy than that of a "free" water molecule. According to a recent computer simulation, a water molecule "bound" to a micelle is stabilized by about 8 kcal mol^{-1} compared to bulk (free) water (Fig. 7).[38] In this model, the rate-determining step in solvation dynamics is the rate of inter-conversion of bound-to-free water (k_{bf}),[9]

$$k_{bf} = \left(\frac{k_B T}{h}\right) \exp\left(\frac{-(\Delta G^0 + \Delta G^*)}{RT}\right), \quad (2)$$

where, ΔG^* is the activation energy for the conversion of free-to-bound water molecules.

In an attempt to verify this model, Sen et al.[39] studied temperature dependence of solvation dynamics in a micelle, triton X-100 (TX-100). They found that with rise in temperature solvation time in TX-100 micelle decreases. The average solvation times are found to be 800, 400, and 110 ps at 283, 303, and 323 K, respectively. According to Eq. 2, the plot of logarithm of average solvation time against $1/T$ should be linear. Such a linear plot has been observed for TX-100 micelle,[39] a cyclodextrin aggregate[40] and in a protein.[41] In the case of TX-100 micelle, from such a plot the activation energy is found to be 9 ± 1 kcal mol^{-1} with a positive entropy factor of 14 cal K^{-1} mol^{-1}.[39] It is interesting to note that the activation energy obtained experimentally from temperature dependence of solvation dynamics is very close to the energy difference between bound and free water, estimated in a computer simulation.[38] In the case of a cyclodextrin aggregate, the average solvation time decrease dramatically from 660 to 30 ps with increase in temperature from 278 to 318 K (Fig. 8).[40] This corresponds to an activation barrier of 12.5 kcal mol^{-1} and an entropy of activation of 28 cal mol^{-1} K^{-1}. Solvation dynamics of 8-anilino-1-naphthalenesulfonate (ANS) bound to bovine serum albumin (BSA) displays a component (300 ps) which is independent of temperature in the range of 278–318 K and a long component which decreases from 5800 ps at 278 K to 3600 ps at 318 K.[41] The temperature independent part (300 ps

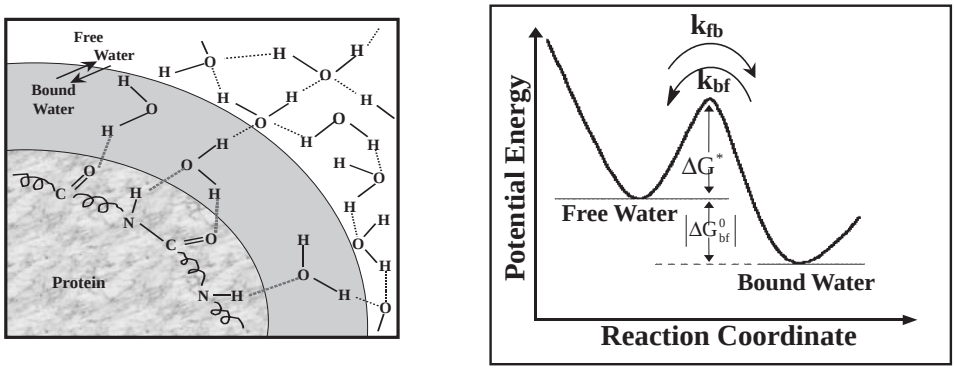

Fig. 7. (a) Free and bound water in the hydration shell of a protein. (b) Dynamic exchange model (Reprinted with permission from Ref. 6. Copyright © 2003 American Chemical Society).

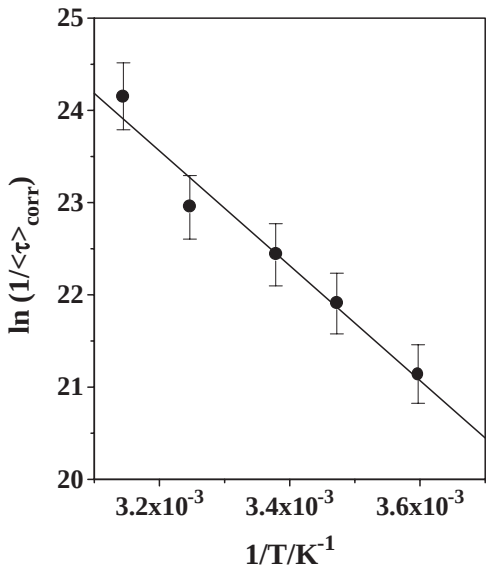

Fig. 8. Plot of $\ln(1/\langle\tau_s\rangle_{corr})$ against $1/T$ for C153 in 40 mM γ-CD (Reprinted with permission from Ref. 40. Copyright © 2005 American Chemical Society).

component) is ascribed to a dynamic exchange of bound to free water with a low barrier. The temperature variation of the long component of solvation dynamics corresponds to an activation energy of 2.1 kcal mol^{-1}. The activation energy is ascribed to local segmental motion of the protein along with the associated water molecules and polar residues. The entropy of activation is found to be -13 cal K^{-1} mol^{-1}. The observed negative entropy suggests an ordering of the local structure at the transition state of the protein segment during dipolar relaxation.[41]

3. Proton and Electron Transfer in a Confined System

In a polar reaction, a non-polar reactant is converted into a charge-separated species. The most common example of such a reaction is dissociation of an acid into proton and anion and also electron-transfer reactions. Solvation makes a polar reaction more facile. We will now discuss ultrafast excited state proton- and electron-transfer processes inside a nano-cavity. We will show that in an organized environment ultraslow solvation and unfavorable geometry causes marked retardation of polar proton and electron-transfer processes.

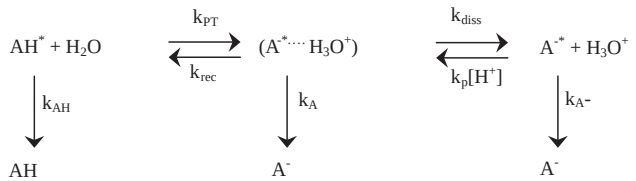

Scheme 1. Proton-transfer processes in pyranine.

3.1 Excited State Proton-Transfer Processes. Acidity of many molecules markedly increases in the excited state. For instance, pK_a of HPTS (8-hydroxypyrene-1,3,6-trisulfonate, HPTS) decreases from 7.4 in the ground state to 0.4 in the first excited state.[42] Thus in the excited state, acidity of HPTS is ≈10-million times stronger than that in the ground state and hence, an excited HPTS rapidly transfers a proton to a water molecule even in a highly acidic media (e.g. pH ≈1).

Excited state proton transfer (ESPT) in an organized assembly differs markedly from that in bulk water. The local pH or pK_a of the acid may be very different from those in the bulk because of the differences in polarity and presence of counter ion and consequent, electrostatic interactions. pH at the surface of a cationic micelle (CTAB) has been determined using HPTS as a probe.[43] It is observed that at a bulk pH 7, the pH at the surface of CTAB micelle is ≈9.5.

ESPT from HPTS to water involves three basic steps—proton transfer (k_{PT}), recombination (k_{rec}), and dissociation (k_{diss}) of the geminate ion pair (Scheme 1). In the reactive stage, a fast short range charge separation occurs and a solvent stabilized ion pair is formed. The next step is the geminate recombination of the ion pair. Confinement of the acid slows down the initial dissociation because of ultraslow solvent response and accelerates the recombination of the geminate ion-pair because of close proximity. Mondal et al. investigated ESPT of HPTS in γ-cyclodextrin (γ-CD) cavity using picosecond and femtosecond fluorescence spectroscopy.[44] They showed that the recombination of the geminate ion pair accelerates but the initial proton-transfer step and the dissociation of the geminate ion pair slow down inside γ-CD. Sahu et al. showed that deprotonation, recombination, and dissociation of the geminate ion pair in the lysozyme–CTAB aggregate are faster than that

in a CTAB micelle.[45]

ESPT from HPTS to acetate in bulk water may be monitored by the rise of the carbonyl IR band at 1720 cm^{-1} arising from acetic acid.[46–48] The rise of this band clearly monitors arrival of the proton to the acetate ion. Two different time constants have been observed for ESPT to acetate. For those HPTS which are hydrogen bonded to the acetate ion in the ground state, ESPT occurs in <150 fs (0.15 ps). For complexes where HPTS and acetate are separated by water molecules, the overall proton-transfer time is 6 ps and is likely to occur through a Grotthuss-type proton transfer.[49] Mohammed et al. showed that proton transfer from HPTS to mono-chloroacetate ($ClCH_2COO^-$) in D_2O involve "loose complexes" with D_2O bridges separating HPTS and $ClCH_2COO^-$.[48]

At the surface of the micelle,[43] emission of HPTS is quenched by acetate ion with a bimolecular quenching constant, $3.5 \times 10^7\ M^{-1}\ s^{-1}$. This is markedly slower than ESPT in a solvent-separated HPTS–water–acetate complex in bulk water. It is interesting to note that even at very high local concentration of acetate (≈7.75 M) in the Stern layer, the rate of proton transfer from HPTS to acetate occurs in 1300–2050 ps time scale.[43] This is an order of magnitude slower than the time constant (6 ps)[49] of ESPT in solvent-separated HPTS–water–acetate system in bulk water. The slow ESPT at the micellar surface compared to bulk water may be ascribed to following. First, the rigidity of water hydrogen-bond network in the Stern layer of the micelle slows down ESPT. Second, at the surface of a micelle surfactant chains may get inserted between HPTS and acetate and thus prevents direct ultrafast proton transfer.

ESPT from HPTS to acetate inside a γ-cyclodextrin (γ-CD) and a *O*-hydroxypropyl γ-nanocavity (Hp-γ-CD) is found to be much slower than that in bulk water.[50] A simple molecular modeling indicates that in the γ-CD:HPTS:acetate complex, the acetate group is not directly hydrogen bonded to the OH group of HPTS (distance ≈4 Å).[50] Instead, the acetate group remains hydrogen bonded to the two OH groups of the γ-CD. The OH group of HPTS is found to be hydrogen bonded to an OH group of γ-CD. This OH group is not hydrogen bonded to the acetate. The OH group of HPTS is also hydrogen bonded to two water molecules which are hydrogen-bonded to the acetate group. In other words, inside the γ-CD cavity the acetate is separated from the OH group of HPTS by two water molecules as bridges.[50] In this case, proton transfer from HPTS to acetate is not direct and is mediated by water bridges and thus resembles the Grotthuss mechanism. Obviously, in the cavity ESPT from HPTS to acetate requires rearrangement of the hydrogen-bond network and the cyclodextrin cavity. In 40 mM γ-CD, the rate of initial proton-transfer process (k_{PT}) increases ≈3 times from $4.0 \pm 0.4 \times 10^{-3}\ ps^{-1}$ at 0 M acetate to $11 \pm 2.0 \times 10^{-3}\ ps^{-1}$ at 2 M acetate.[50] In contrast, in the case of Hp-γ-CD the initial proton-transfer rate (k_{PT}) remains almost unaffected on addition of acetate. It seems that the hydroxypropyl group of Hp-γ-CD shields the encapsulated HPTS molecule from the acetate. Hence, it is more difficult for the acetate to access HPTS in Hp-γ-CD than in unsubstituted γ-CD.[50] As a result, ESPT in Hp-γ-CD is much slower.

3.2 Photoinduced Electron Transfer. Photoinduced electron transfer (PET) plays a fundamental role in many chemical and biological processes.[51] PET involves transfer of an electron from an electron donor to an excited dye molecule. In an organized assembly, the donor and the acceptor reside at a close distance and hence PET is expected to be faster than that in bulk solvent. An implicit assumption of the Marcus theory is that solvation is very fast and at each point along the reaction coordinate the solvent reorganizes in a time scale faster than electron-transfer rate.[51] The classical Marcus model predicts a bell-shaped dependence of rate of ET on the free-energy change.[51] Yoshihara and co-workers first reported that in liquid DMA (*N*,*N*-dimethylaniline) PET exhibits a component faster than the solvation time.[52–54] Interestingly, even for ultrafast PET, they observed a bell-shaped dependence of PET rate on free-energy change (ΔG) and thus detected the so called Marcus inverted region.[52–54] Bagchi and Gayathri developed a non-Markovian model and correlated the highly non-exponential ET process with the highly non-exponential solvation dynamics.[55] They noted that in most solvents, the solvation dynamics consist of an ultrafast sub-picosecond inertial component and a slower component in tens of picosecond. They showed that 30–40% solvent relaxation is enough to bring about the ultrafast electron transfer observed by Yoshihara and co-workers.[52–54]

Barbara and Olson proposed a modified model which includes a classical low frequency vibration, a classical solvent coordinate (X), and a high frequency quantum mode.[56] In a seminal paper, Sumi and Marcus introduced an irreversible stochastic model of ET with a wide sink term.[57] This led to the so called 2D-ET model. This model involves a solvent polarization coordinate (X) and a low frequency classical vibrational coordinate (Q). According to this model, the relaxation along Q is much faster than that along X and the effect of Q is included using a position-dependent rate constant, $k(X)$.[57]

Tachiya and co-workers carried out a detailed calculation of solvent reorganization energy and free-energy change in a micelle.[58,59] They showed that the rate of PET increases with the increase of the chain length of the surfactant.[58,59] It is obviously of interest to find out how PET is influenced by the slow solvation dynamics and proximity of the donor and acceptor, in a nanocavity.

In a micelle[60–62] or inside a cyclodextrin cavity,[63] the donor (DMA) and the acceptor (coumarin dyes) stay very close and hence, PET in a micelle is expected to be almost as fast as that in neat DMA. Ghosh et al. detected ultrafast components (<10 ps) of PET in a micelle[62] and in a *O*-hydroxypropyl γ-cyclodextrin cavity[63] using a femtosecond up-conversion set up. For C481, C153, and C151, PET is found to be faster than solvation dynamics and hence, no rise is observed at the red end in the presence of the quencher. However, for C480 the fluorescence transient continues to exhibit a rise even at the highest concentration of the donor (DMA).[62,63] This suggests that a part of solvation dynamics is slower than rate of PET in C480. In both the cases, a bell-shaped dependence of ultrafast PET on the free energy change (Fig. 9) is observed which is similar to Marcus inversion.[62,63]

Most recently, Eisenthal and McArthur reported ultrafast dynamics of PET at DMA/water interface using femtosecond pump–probe surface SHG.[64] They detected the time constants of both forward and back electron transfer from time-resolved surface SHG resonant for the $DMA^{+\bullet}$ radical.[64]

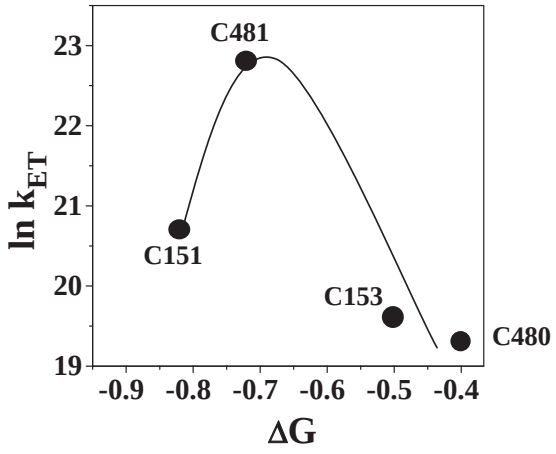

Fig. 9. The $\ln k_{ET}$ vs ΔG plot for coumarin–DMA system in 50 mM *O*-hydroxypropyl γ-cyclodextrin (Reprinted with permission from Ref. 63. Copyright © 2006 American Chemical Society).

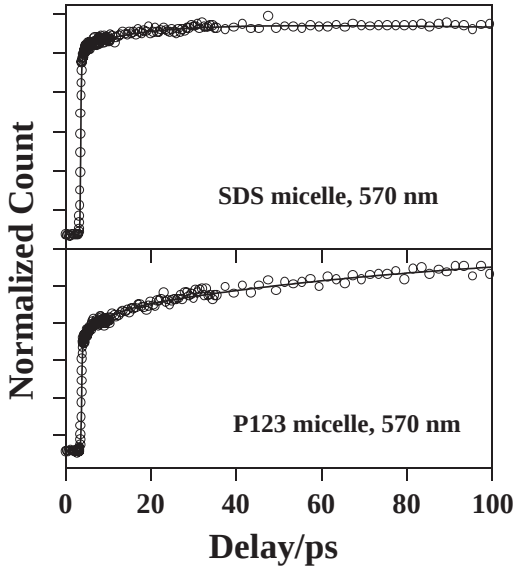

Fig. 10. Femtosecond rise of the acceptor (R6G) in SDS and P123 micelle ($\lambda_{ex} = 405$ nm and $\lambda_{em} = 570$ nm) (Reprinted with permission from Ref. 69. Copyright © 2006 American Physical Society).

4. Fluorescence Resonance Energy Transfer

Fluorescence resonance energy transfer (FRET) inside an organized assembly is expected to be much faster than that in bulk water because of proximity of the donor and the acceptor. At a very short D–A distance, the electron clouds of donor and acceptor may overlap and basic assumptions of Forster theory (product wavefunctions and point-dipole approximation) may not be valid.[65,66]

FRET between a donor and an acceptor both enclosed in the same micelle is a simple system to study ultrafast FRET at a short distance. Sarkar and co-workers studied energy transfer from several coumarin dyes (C480, C151, and C153) to rhodamine 6G (R6G) in non-aqueous reverse micelles.[67] They found a very large discrepancy in the efficiency of FRET estimated from the steady state emission intensity and picosecond measurement of lifetime of the donor. The discrepancy may be reconciled as follows. In most of the micelles, only the donor is present which do not participate in FRET. In this case, the decay recorded in a picosecond set up is dominated by the unquenched donors and hence, no shortening of the donor lifetime is detected.[68] For the donors with an acceptor in the immediate vicinity in the same micelle, the emission is strongly quenched and the lifetime becomes too short to be detected in a picosecond set up. The ultrafast component of the decay (arising from FRET) of these set of donors is missed in a picosecond set up.

The time constants of FRET may be correctly determined if one studies the rise time of the acceptor emission (Fig. 10) using a femtosecond set up.[69] Using this approach, two ultrafast components (0.7 and 13 ps) of FRET are detected in a small SDS (core radius $\approx$20 Å) micelle. These two components correspond to Forster distances (R_{DA})—12 and 19 Å, respectively.[69] In the big P123 micelle (core radius $\approx$50 Å) in addition to the ultrafast components (1.2 and 24 ps), a long component of 1000 ps is observed.[69] The long component (1000 ps) corresponds to a $R_{DA} = 44$ Å. The R_{DA} calculated from the ultrafast component is roughly equal to the donor–acceptor distance for direct contact and the R_{DA} calculated from the long component agrees well with micellar radius.[69]

Mondal et al. studied λ_{ex} dependence of FRET in AOT reverse micelle using C480 as donor and Fluorescein 548 (F548) as acceptor.[70] The anionic acceptor resides inside the water pool while the donor (C480) is distributed over three locations—bulk heptane, AOT interface, and the core of the water pool. They observed that FRET occurs inside AOT microemulsion in three time scales—3, 200, and 2700 ps. The 3 ps component is assigned to FRET in the water pool of the reverse micelle at a donor–acceptor distance 16 Å. The 200 ps component corresponds to a donor–acceptor distance 30 Å and is ascribed to the negatively charged acceptor inside the water pool and the neutral donor inside the alkyl chains of AOT. The very long 2700 ps component arises from diffusion of the donor from bulk heptane to the reverse micelle. At $\lambda_{ex} = 375$ nm, C480 molecules in the bulk heptane are preferentially excited. At $\lambda_{ex} = 405$ nm, C480 inside the reverse micelle are excited. As a result, with increase in the excitation wavelength from 375 to 405 nm the relative contribution of the FRET due to C480 in the AOT reverse micelle (3 and 200 ps components) increases.[70]

5. Fluorescence Anisotropy Decay

The time-dependent fluorescent anisotropy is given by

$$r(t) = \frac{I_{\parallel}(t) - GI_{\perp}(t)}{I_{\parallel}(t) + 2GI_{\perp}(t)}, \quad (3)$$

where G is a correction factor arising from the anisotropic response of the instrument. $I_{\parallel}(t)$ and $I_{\perp}(t)$ are time-dependent emission intensities polarized, respectively parallel and perpendicular to the polarization of the exciting light pulse.

Sen et al. measured anisotropy decay of C153 inside di- and tri-methyl β-CD.[13] They observed a bi-exponential decay with components 1000–1150 and 2500–2700 ps. They ascribed the components respectively to the 1:1 and 1:2 complex of C153

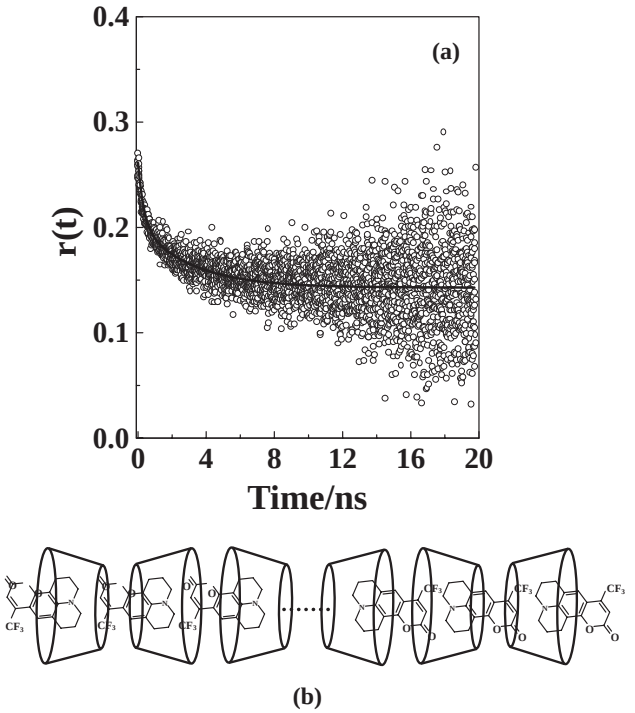

Fig. 11. (a) Fluorescence anisotropy decay of C153 ($\lambda_{ex} =$ 405 nm and $\lambda_{em} = 490$ nm) in 40 mM γ-CD at 278 K. (b) Model of C153: γ-CD linear aggregate (Reprinted with permission from Ref. 40. Copyright © 2005 American Chemical Society).

with cyclodextrin (Fig. 1). The hydrodynamic radius (r_h) of the complexes may be estimated from the time constant (τ_R) of fluorescence anisotropy decay using the equation

$$\tau_R = \frac{4\pi\eta r_h^3}{3kT}. \quad (4)$$

The hydrodynamic radius of the 1:1 and 1:2 complexes are 8.5 ± 0.5 and 11.5 ± 0.5 Å, respectively. Since the height of dimethyl β-CD is 10.9 Å.[10] This suggests that ≈5 Å the probe is projected out of the cavity in case of the 1:1 complex. The hydrodynamic diameter ($2r_h$) of 1:2 complex is roughly equal to the sum of height of two CD cavities.[13]

Most recently, Roy et al. observed an extremely slow anisotropy decay (time constant >20 ns) for the C153-γ-cyclodextrin guest–host complex (Fig. 11).[40] They attributed the ultraslow time constant of anisotropy to the formation of a long nano-tube aggregates containing a large number (>50) cyclodextrins joined together non-covalently through the guest molecules (Fig. 11).[40]

6. Conclusion

In a confined system, disruption of the water–water hydrogen-bond network, immobilization of the water molecules because of binding with macromolecules and close proximity affect the dynamics profoundly. This leads to both ultrafast and ultraslow dynamics. As shown in this article, dynamics in a nano-confined system is fundamentally different from that in a bulk liquid. The recent results on these systems have implications in many biological processes. Recent progress in this area raised the hope that in near future, it will be possible to unravel dynamics of biological systems in minute details. The ultimately goal of such a study is to understand the relation between dynamics and biological function.

Thanks are due to Department of Science and Technology, India (Project Number: IR/I1/CF-01/2002) and Council of Scientific and Industrial Research (CSIR) for generous research grants. KS, SKM, and SG thank CSIR for awarding fellowships. KB thanks Professors B. Bagchi, K. Tominaga, and T. Tahara for many stimulating discussions and useful collaborations.

References

1 W. Jarzeba, G. C. Walker, A. E. Johnson, M. A. Kahlow, P. F. Barbara, *J. Phys. Chem.* **1988**, *92*, 7039.
2 R. Jimenez, G. R. Fleming, P. V. Kumar, M. Maroncelli, *Nature* **1994**, *369*, 471.
3 N. Nandi, S. Roy, B. Bagchi, *J. Chem. Phys.* **1995**, *102*, 1390.
4 C. J. Fecko, J. D. Eaves, J. J. Loparo, A. Tokmakoff, P. L. Geissler, *Science* **2003**, *301*, 1698.
5 N. Nandi, B. Bagchi, K. Bhattacharyya, *Chem. Rev.* **2000**, *100*, 2013.
6 K. Bhattacharyya, *Acc. Chem. Res.* **2003**, *36*, 95.
7 B. Bagchi, *Chem. Rev.* **2005**, *105*, 3197.
8 S. K. Pal, A. H. Zewail, *Chem. Rev.* **2004**, *104*, 2099.
9 N. Nandi, B. Bagchi, *J. Phys. Chem. B* **1997**, *101*, 10954.
10 K. Uekama, F. Hirayama, T. Irie, *Chem. Rev.* **1998**, *98*, 2045.
11 M. Khajehpour, T. Troxler, V. Nanda, J. M. Vanderkooi, *Proteins* **2004**, *55*, 275.
12 S. Vajda, R. Jimenez, S. J. Rosenthal, V. Fidler, G. R. Fleming, E. W. Castner, Jr., *J. Chem. Soc., Faraday Trans.* **1995**, *91*, 867.
13 P. Sen, D. Roy, S. K. Mondal, K. Sahu, S. Ghosh, K. Bhattacharyya, *J. Phys. Chem. A* **2005**, *109*, 9716.
14 A. P. Demchenko, *Biophys. Chem.* **1982**, *15*, 101.
15 J. R. Lakowicz, *Biochemistry* **1984**, *23*, 3013.
16 D. A. Kelkar, A. Chattopadhyay, *J. Phys. Chem. B* **2004**, *108*, 12151.
17 T. Satoh, H. Okuno, K. Tominaga, K. Bhattacharyya, *Chem. Lett.* **2004**, *33*, 1090.
18 P. Sen, T. Satoh, K. Bhattacharyya, K. Tominaga, *Chem. Phys. Lett.* **2005**, *411*, 339.
19 P. Sen, S. Ghosh, S. K. Mondal, K. Sahu, D. Roy, K. Bhattacharyya, K. Tominaga, *Chem. Asian J.* **2006**, *1*, 188.
20 P. Sen, S. Ghosh, K. Sahu, S. K. Mondal, D. Roy, K. Bhattacharyya, *J. Chem. Phys.* **2006**, *124*, 204905.
21 S. Guha, K. Sahu, D. Roy, S. K. Mondal, S. Roy, K. Bhattacharyya, *Biochemistry* **2005**, *44*, 8940.
22 K. Chattopadhyay, S. Mazumdar, *Biochemistry* **2003**, *42*, 14606.
23 K. Sahu, S. K. Mondal, S. Ghosh, D. Roy, P. Sen, K. Bhattacharyya, *J. Phys. Chem. B* **2006**, *110*, 1056.
24 S. Samaddar, A. K. Mandal, S. K. Mondal, K. Sahu, K. Bhattacharyya, S. Roy, *J. Phys. Chem. B* **2006**, *110*, 21210.
25 P. Sen, D. Roy, K. Sahu, S. K. Mondal, K. Bhattacharyya, *Chem. Phys. Lett.* **2004**, *395*, 58.
26 K. Sahu, S. K. Mondal, D. Roy, R. Karmakar, K. Bhattacharyya, *Chem. Phys. Lett.* **2005**, *413*, 484.
27 S. Bandyopadhyay, S. Chakraborty, B. Bagchi, *J. Am.*

Chem. Soc. **2005**, *127*, 16660.
28 S. Bandyopadhyay, S. Chakraborty, S. Balasubramanian, B. Bagchi, *J. Am. Chem. Soc.* **2005**, *127*, 4071.
29 S. Abel, M. Waks, W. Urbach, M. Marchi, *J. Am. Chem. Soc.* **2006**, *128*, 382.
30 A. A. Hassanali, T. P. Li, D. P. Zhong, S. J. Singer, *J. Phys. Chem. B* **2006**, *110*, 10497.
31 U. Heugen, G. Schwaab, E. Brundermann, M. Heyden, X. Yu, D. M. Leitner, M. Havenith, *Proc. Natl. Acad. Sci. U.S.A.* **2006**, *103*, 12301.
32 C. Caronna, F. Natali, A. Cupane, *Biophys. Chem.* **2005**, *116*, 219.
33 D. Russo, R. K. Murarka, J. R. D. Copley, T. Head-Gordon, *J. Phys. Chem. B* **2005**, *109*, 12966.
34 K. Modig, E. Liepinsh, G. Otting, B. Halle, *J. Am. Chem. Soc.* **2004**, *126*, 102.
35 S. K. Pal, L. Zhao, T. Xia, A. H. Zewail, *Proc. Natl. Acad. Sci. U.S.A.* **2003**, *100*, 13746.
36 D. Andreatta, J. L. P. Lustres, S. A. Kovalenko, N. P. Ernsting, C. J. Murphy, R. S. Coleman, M. A. Berg, *J. Am. Chem. Soc.* **2005**, *127*, 7270.
37 D. Andreatta, S. Sen, J. L. P. Lustres, S. A. Kovalenko, N. P. Ernsting, C. J. Murphy, R. S. Coleman, M. A. Berg, *J. Am. Chem. Soc.* **2006**, *128*, 6885.
38 S. Pal, S. Balasubramanian, B. Bagchi, *J. Phys. Chem. B* **2003**, *107*, 5194.
39 P. Sen, S. Mukherjee, A. Halder, K. Bhattacharyya, *Chem. Phys. Lett.* **2004**, *385*, 357.
40 D. Roy, S. K. Mondal, K. Sahu, S. Ghosh, P. Sen, K. Bhattacharyya, *J. Phys. Chem. A* **2005**, *109*, 7359.
41 K. Sahu, S. K. Mondal, S. Ghosh, D. Roy, P. Sen, K. Bhattacharyya, *J. Chem. Phys.* **2006**, *124*, 124909.
42 K. K. Smith, K. J. Kaufmann, D. Huppert, M. Gutman, *Chem. Phys. Lett.* **1979**, *64*, 522.
43 D. Roy, R. Karmakar, S. K. Mondal, K. Sahu, K. Bhattacharyya, *Chem. Phys. Lett.* **2004**, *399*, 147.
44 S. K. Mondal, K. Sahu, P. Sen, D. Roy, S. Ghosh, K. Bhattacharyya, *Chem. Phys. Lett.* **2005**, *412*, 228.
45 K. Sahu, D. Roy, S. K. Mondal, R. Karmakar, K. Bhattacharyya, *Chem. Phys. Lett.* **2005**, *404*, 341.
46 M. Rini, B.-Z. Magnes, E. Pines, E. T. J. Nibbering, *Science* **2003**, *301*, 349.
47 M. Rini, D. Pines, B.-Z. Magnes, E. Pines, E. T. J. Nibbering, *J. Chem. Phys.* **2004**, *121*, 9593.
48 O. Mohammed, D. Pines, J. Dryer, E. Pines, E. T. J. Nibbering, *Science* **2005**, *310*, 83.
49 N. Agmon, *J. Phys. Chem. A* **2005**, *109*, 13.
50 S. K. Mondal, K. Sahu, S. Ghosh, P. Sen, K. Bhattacharyya, *J. Phys. Chem. A* **2006**, *110*, 13646.
51 R. A. Marcus, *Advances in Chemical Physics*, **1999**, Vol. 106, p. 1.
52 K. Yoshihara, *Advances in Chemical Physics*, **1999**, Vol. 107, p. 371.
53 H. Pal, Y. Nagasawa, K. Tominaga, K. Yoshihara, *J. Phys. Chem.* **1996**, *100*, 11964.
54 H. Shirota, H. Pal, K. Tominaga, K. Yoshihara, *J. Phys. Chem. A* **1998**, *102*, 3089.
55 B. Bagchi, N. Gayathri, *Advances in Chemical Physics*, **1999**, Vol. 107, p. 1.
56 P. F. Barbara, E. J. J. Olson, *Advances in Chemical Physics*, **1999**, Vol. 107, p. 647.
57 H. Sumi, R. A. Marcus, *J. Chem. Phys.* **1986**, *84*, 4894.
58 H. L. Tavernier, A. V. Barzykin, M. Tachiya, M. D. Fayer, *J. Phys. Chem. B* **1998**, *102*, 6078.
59 A. V. Barzykin, K. Seki, M. Tachiya, *J. Phys. Chem. B* **1999**, *103*, 9156.
60 M. Kumbhakar, S. Nath, H. Pal, A. V. Sapre, T. Mukherjee, *J. Chem. Phys.* **2003**, *119*, 388.
61 D. Chakraborty, A. Chakrabarty, D. Seth, N. Sarkar, *Chem. Phys. Lett.* **2003**, *382*, 508.
62 S. Ghosh, K. Sahu, S. K. Mondal, P. Sen, K. Bhattacharyya, *J. Chem. Phys.* **2006**, *125*, 054509.
63 S. Ghosh, S. K. Mondal, K. Sahu, K. Bhattacharyya, *J. Phys. Chem. A* **2006**, *110*, 13139.
64 E. A. McArthur, K. B. Eisenthal, *J. Am. Chem. Soc.* **2006**, *128*, 1068.
65 S. Bhowmick, S. Saini, V. B. Shenoy, B. Bagchi, *J. Chem. Phys.* **2006**, *125*, 181102.
66 C. S. Yun, A. Javier, T. Jennings, M. Fisher, S. Hira, S. Peterson, B. Hopkins, N. O. Reich, G. F. Strouse, *J. Am. Chem. Soc.* **2005**, *127*, 3115.
67 D. Seth, D. Chakrabarty, A. Chakraborty, N. Sarkar, *Chem. Phys. Lett.* **2005**, *401*, 546.
68 G. A. Kenny-Wallace, J. H. Flint, S. C. Wallace, *Chem. Phys. Lett.* **1975**, *32*, 71.
69 K. Sahu, S. Ghosh, S. K. Mondal, B. C. Ghosh, P. Sen, D. Roy, K. Bhattacharyya, *J. Chem. Phys.* **2006**, *125*, 044714.
70 S. K. Mondal, S. Ghosh, K. Sahu, U. Mandal, K. Bhattacharyya, *J. Chem. Phys.* **2006**, *125*, 224710.

Kalyanasis Sahu was born in 1981. He obtained master's degree in chemistry from University of Calcutta in 2003. He is currently doing his Ph.D. at Indian Association for the Cultivation of Science (IACS) under the supervision of Professor Kankan Bhattacharyya.

Sudip Kumar Mondal (b. 1980) studied in Visva-Bharati University and got master's degree in chemistry in 2003. He is carrying out his Ph.D. research at IACS with Professor Kankan Bhattacharyya.

Subhadip Ghosh (b. 1981) received master's degree in chemistry from Vidyasagar University in 2004. He is a research fellow working at IACS with Professor Kankan Bhattacharyya.

Kankan Bhattacharyya (b. 1954) carried out Ph.D. research at IACS and obtained Ph.D. degree in 1984. He was a research associate at the Radiation Laboratory, University of Notre Dame (1984–86) and at Columbia University (1986–87). He joined the faculty of IACS in 1987 and became a professor in 1998. His research interest includes ultrafast laser spectroscopy and organized assemblies.